A&A 525, A101 (2011)
DOI: 10.1051/0004-6361/201014777

Astronomy & Astrophysics

Plaskett's star: analysis of the CoRoT photometric data⋆,⋆⋆

L. Mahy[1], E. Gosset[1,⋆⋆⋆], F. Baudin[2], G. Rauw[1,†], M. Godart[1], T. Morel[1], P. Degroote[3], C. Aerts[3,5], R. Blomme[4], J. Cuypers[4], A. Noels[1], E. Michel[6], A. Baglin[7], M. Auvergne[8], C. Catala[8], and R. Samadi[8]

[1] Institut d'Astrophysique et de Géophysique, University of Liège, Bât. B5C, Allée du 6 Août 17, 4000 Liège, Belgium
e-mail: mahy@astro.ulg.ac.be
[2] Institut d'Astrophysique Spatiale (IAS), Bâtiment 121, 91405 Orsay Cedex, France
[3] Instituut voor Sterrenkunde, K.U. Leuven, Celestijnenlaan 200D, 3001 Leuven, Belgium
[4] Royal Observatory of Belgium, Ringlaan 3, 1180 Brussel, Belgium
[5] Department of Astrophysics, IMAPP, University of Nijmegen, PO Box 9010, 6500 GL Nijmegen, The Netherlands
[6] LESIA, CNRS, Université Pierre et Marie Curie, Université Denis Diderot, Observatoire de Paris, 92195 Meudon Cedex, France
[7] Laboratoire AIM, CEA/DSM-CNRS-Université Paris Diderot, CEA, IRFU, SAp, centre de Saclay, 91191 Gif-sur-Yvette, France
[8] LESIA, UMRR8109, Université Pierre et Marie Curie, Université Denis Diderot, Observatoire de Paris, 92195 Meudon Cedex, France

Received 12 April 2010 / Accepted 22 October 2010

ABSTRACT

Context. The second short run (SRa02) of the CoRoT space mission for asteroseismology was partly devoted to stars belonging to the Mon OB2 association. An intense monitoring has been performed on Plaskett's star (HD 47129) and the unprecedented quality of the light curve allows us to shed new light on this very massive, non-eclipsing binary system.

Aims. We particularly aimed at detecting periodic variability that might be associated with pulsations or interactions between both components. We also searched for variations related to the orbital cycle that could help to constrain the inclination and the morphology of the binary system.

Methods. We applied an iterative Fourier-based prewhitening and a multiperiodic fitting procedure to analyse the time series and extract the frequencies of variations from the CoRoT light curve. We describe the noise properties to tentatively define an appropriate significance criterion and, in consequence, to only point out the peaks at a certain significance level. We also detect the variations related to the orbital motion and study them with the NIGHTFALL programme.

Results. The periodogram computed from Plaskett's star CoRoT light curve mainly exhibits a majority of peaks at low frequencies. Among these peaks, we highlight a list of 43 values, notably including two different sets of harmonic frequencies whose fundamental peaks are located at about 0.07 and 0.82 d^{-1}. The former represents the orbital frequency of the binary system, whilst the latter could probably be associated with non-radial pulsations. The study of the 0.07 d^{-1} variations reveals a hot spot most probably situated on the primary star and facing the secondary.

Conclusions. The investigation of this unique dataset constitutes a further step in the understanding of Plaskett's star. These results provide a first basis for future seismic modelling and put forward the probable existence of non-radial pulsations in Plaskett's star. Moreover, the fit of the orbital variations confirms the problem of the distance of this system which was already mentioned in previous works. A hot region between both components renders the determination of the inclination ambiguous.

Key words. stars: early-type – stars: oscillations – stars: individual: HD 47129 – binaries: general

1. Introduction

Plaskett's star, or HD 47129, has long been considered as one of the most massive binary systems in our Galaxy. For nine decades, this star has not stopped to fascinate by its complexity. It has been the subject of several investigations in different wavelength domains, but despite these efforts, the system is still not fully understood.

Plaskett's star is a non-eclipsing binary (Morrison 1978) composed of two very massive and luminous O-type stars. The secondary component features broad and shallow stellar lines, suggesting that this star rotates rapidly. Its projected rotational velocity has been estimated to be close to 300 km s^{-1}, while that of the primary has been measured at about 75 km s^{-1} (Linder et al. 2008). As a consequence of this high rotation speed, the secondary star probably presents a temperature gradient between the poles and equator that could bias the determination of its spectral type, but most importantly, the secondary has a rotationally flattened wind. This configuration probably accounts for several properties of the wind interaction zone. The study of the Hα region by Wiggs & Gies (1992) and Linder et al. (2008) as well as the analysis of Linder et al. (2006) in the X-ray domain have confirmed this assumption.

Bagnuolo et al. (1992) applied a tomographic technique to the International Ultraviolet Explorer (IUE) data to separate the contribution of the secondary star from the primary's spectrum. Their investigation of the individual spectral components has

⋆ The CoRoT space mission was developed and is operated by the French space agency CNES, with participation of ESA's RSSD and Science Programmes, Austria, Belgium, Brazil, Germany and Spain.

⋆⋆ Table 2 is only available in electronic form at http://www.aanda.org

⋆⋆⋆ Senior Research Associate FRS-FNRS.

† Research Associate FRS-FNRS.

provided the spectral types of O7.5 I and O6 I for the primary and secondary stars, respectively, and a mass ratio of M_2/M_1 = 1.18 ± 0.12. Assuming an inclination of 71 ± 9° as estimated by Rudy & Herman (1978) from polarimetry, they found masses equal to 42.5 $M_\odot$ for the primary and 51.6 $M_\odot$ for the secondary.

Linder et al. (2008) found from high-resolution optical spectra minimum masses of 45.4 and 47.3 $M_\odot$ for the primary and secondary, respectively, implying a mass ratio of about 1.05 ± 0.05. They also disentangled the spectra by using an algorithm based on the method of González & Levato (2006). The individual spectra indicated an O8 III/I+O7.5 V/III binary system. In addition, these authors used the model atmosphere code CMFGEN (Hillier & Miller 1998) to derive the wind and the photospheric properties of both components. The major point of their study is the confirmation of an N overabundance and a C depletion of the primary star, which provides additional proof for a binary system in a post-Roche lobe overflow evolutionary stage where matter has been transferred from the primary to the secondary star.

The most disturbing point concerning Plaskett's star however is the discrepancy between the luminosity of both components and their dynamical masses. Linder et al. (2008) explained that these stars have spectral types that are too late for their masses. A solution to this problem is to assume a larger distance of the star, although this would imply that Plaskett's star does not belong to the Mon OB2 association. Despite the numerous investigations undertaken to probe the physics of this binary system and its components, Plaskett's star still hides part of a mystery.

Even though Reese et al. (2009) have emphasized the difficulty to detect pulsation modes in rapidly rotating stars, there are some examples of rapidly rotating O stars (ζ Oph, Kambe et al. 1997; HD 93521, Howarth & Reid 1993; Rauw et al. 2008) where spectroscopic and photometric variability, which are probably related to non-radial pulsation modes with periods of a few hours, have been identified. These rapid rotators have properties quite reminiscent of those of the secondary component in Plaskett's star, which also displays line profile variability (Linder et al. 2008), although the existing spectroscopic data of the system are too scarce to characterize these variations properly. Asteroseismology could therefore provide new insight into the properties of the components of Plaskett's star.

For this purpose, but also to further constrain the binary system itself, Plaskett's star has been chosen as one of the CoRoT (Convection, Rotation and planetary Transits, Baglin et al. 2006; Auvergne et al. 2009) satellite targets in the Asteroseismology field. The unprecedented quality of the CoRoT light curve clearly allows us to search for variations linked to the orbital period of the system and to determine the possible existence of very low-amplitude variations caused by the presence of radial and non-radial pulsation modes for instance.

The present paper describes a complete and detailed analysis of the light curve of Plaskett's star observed by the CoRoT satellite. We organize it as follows. In Sect. 2 we present the CoRoT data. Section 3 is devoted to the frequency analysis and to a study of the noise properties of the data. In Sect. 4 we discuss the inclination of the binary system and some other results obtained from the analysis of the light curve. Finally, we set forth our conclusions in Sect. 5.

2. The CoRoT data

Plaskett's star was observed during the second CoRoT short run SRa02 pointing towards the anticentre of the Galaxy. The observations were made between 2008 October 08

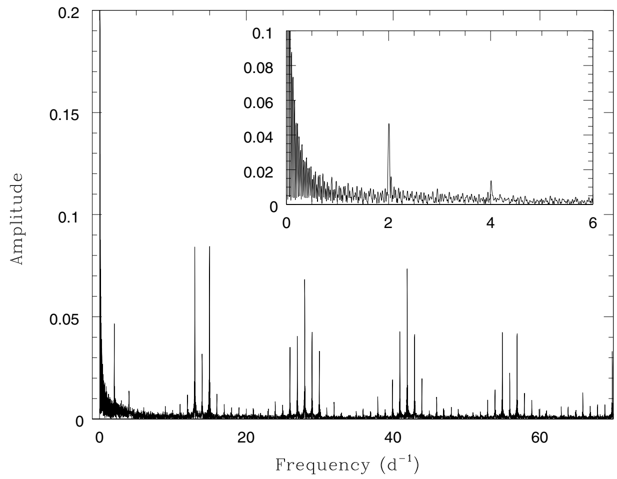

Fig. 1. Spectral window of the final version of the Plaskett's star light curve, observed during the second short run of the mission.

(HJD = 2 454 748.485467) and 2008 November 12 (HJD = 2 454 782.819956). Hereafter, we will express the date as HJD – 2 450 000. The time series obtained is spread over ΔT = 34.334489 days, with a sampling of one point every 32 s. This involves a frequency resolution of $1/\Delta T$ = 0.029125 d^{-1}.

The raw light curve of Plaskett's star contains 92 696 points. At first, we discarded flagged points potentially corrupted by the instrumental conditions (e.g., the changes of CCD masks or the generation of outliers). These observations represent about 4.2% of the datapoints of the CoRoT light curve of Plaskett's star. In addition, we searched the CoRoT light curve for possible jumps or discontinuities caused by a change of the CCD temperature and corrected all of them. Secondly, we also discarded the flagged points associated with the environmental perturbations of the satellite that are mainly due to the regular passage through the South Atlantic Anomaly (SAA) and other Earth orbit perturbations (Auvergne et al. 2009). Because this passage occurs twice in a sidereal day, the spectral window (see the inset in Fig. 1) presents a structure composed of a first peak (4.6% of the amplitude) close to 2.007 d^{-1} and a second one (1.4% of the amplitude) close to 4.014 d^{-1}. Moreover, gaps owing to the orbital period of the satellite (6184 s) produce other structures with peaks around 13.972 d^{-1} and their harmonics (Fig. 1). The percentage of lost datapoints because of environmental conditions is only 9.6% for HD 47129. In addition, the spectral window exhibits a 89.0% peak at f = 2699.764 d^{-1}. This corresponds to the sampling regularity with the highest frequency. Consequently, a pseudo-Nyquist frequency can be located at $f_{\rm Ny}$ = 1349.882 d^{-1} (leading to a step of 32.003 s). We use the word "pseudo" to point out that the aliasing is not pure.

An interpolation of all flagged points of the light curve to fill the gaps cleans the spectral windows of all these peaks, but this process introduces systematic effects that could generate erroneous values of the frequencies and affect the scientific results. Accordingly, we decided not to interpolate among the remaining points of the light curve.

All stars observed in the CoRoT field of view present a global slope in their light curve with probably an instrumental origin (Auvergne et al. 2009, attributed this drift to the ageing of the CCDs). Even though the light curve of Plaskett's star does not seem to be affected by it, maybe because of its high flux variability, we decided to remove this long-term trend. In order not to bias the possible orbital or long-term variations present

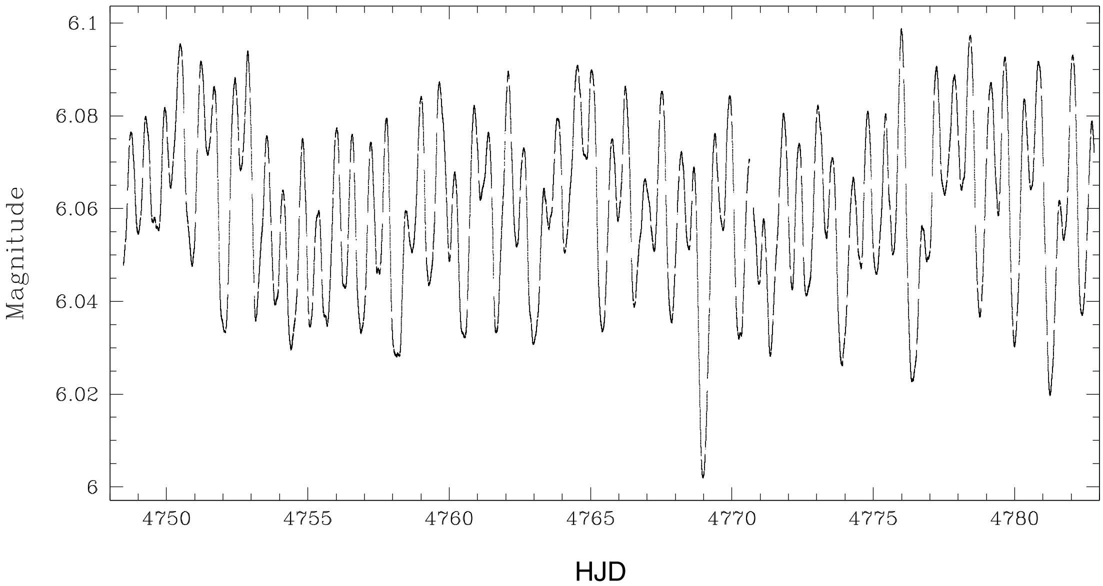

Fig. 2. Full detrended CoRoT light curve of Plaskett's star, containing 79 896 points, observed over about 34.33 days and converted to magnitude. All gaps present in the data are due to the flagged points described in Sect. 2.

in the light curve, the strictly linear trend appears to be the best choice among the different possible trends. However, as we will show in Sect. 3, the low frequencies close to 0 still appear in the semi-amplitude spectrum after removing the trend.

Finally, the CoRoT light curve has also been converted to magnitude from the expression $m = -2.5\log(F) + C$ where F gives the CoRoT flux expressed in $e^{-}\,s^{-1}$ and C represents a calibration constant. We estimated this constant at a value of 23.09 ± 0.01 mag after comparing the CoRoT magnitude to that in the V-band quoted by Linder et al. (2008). We note that this conversion in magnitude does not change the decomposition in frequencies reported below. The final version of Plaskett's star light curve (Fig. 2) is composed of 79 896 points.

3. Analysis of Plaskett's star CoRoT light curve

3.1. Looking for periodic structures

The CoRoT light curve confirms that Plaskett's star is not an eclipsing binary although we detect variations that could be linked to the orbital motion of the binary system ($P_{\rm orb}$ = 14.39625 days, see Linder et al. 2008). The light curve also presents large amplitude peak-to-peak variations on shorter time scales. In order to perform a complete investigation of the frequencies present in the CoRoT light curve, we applied a Fourier analysis based on the Heck et al. (hereafter HMM) technique (Heck et al. 1985; revised by Gosset et al. 2001). We emphasize that this method is comparable to the Ferraz-Mello one (Ferraz-Mello 1981) and is especially designed to handle time series with unevenly spaced data. Moreover, its mathematical expression for the power spectrum has the advantage of correcting some deficiencies of other methods such as the one of Scargle (1982). The Fourier technique of HMM used here is equivalent at each individual frequency to a least-squares fit of a sine function (Gosset et al. 2001). In the present paper we will actually use the semi-amplitude spectrum instead of the classical power spectrum, which means that the ordinates represent the amplitude term in front of the sine function.

The semi-amplitude spectrum (Fig. 3) clearly shows that most of the power is concentrated in the $f \leq 6.0$ d^{-1} frequency domain and that aliases generated by the satellite orbital cycle are present between 11.0 and 17.0 d^{-1}. Although we removed the linear trend from the dataset, the signal remains close to the frequency 0.0 d^{-1}. The spectrum is dominated by a set of frequencies distributed according to a regular pattern including the fundamental frequency at about 0.82 d^{-1} and its possible harmonics at about 1.64 d^{-1}, 2.46 d^{-1}, 3.28 d^{-1} and 4.10 d^{-1}. The 2.007 d^{-1} aliases of the two first (main) frequencies are also visible at f = 2.83 d^{-1} and 3.65 d^{-1}. Besides these frequencies, the semi-amplitude spectrum confirms the presence of f = 0.07 d^{-1}, f = 0.14 d^{-1} and probably f = 0.21 d^{-1}, i.e., the orbital frequency and its harmonics, which constitute a second set of frequencies. Further outstanding peaks are also present at $f \sim 0.35$ d^{-1}, $f \sim 0.65$ d^{-1} and $f \sim 0.95$ d^{-1}. The first one has a wider peak that expected from the time basis, it could actually be a blend of several frequencies (at least two, or one plus an alias of f = 1.64 d^{-1}).

In order to analyse the time series in a more systematic way, the in-depth determination of the different frequencies was done in two steps. First, we proceeded to a classical iterative prewhitening of the signal, frequency by frequency. At each step, the semi-amplitude spectrum is computed and the frequency value is selected by the position of the highest peak in the spectrum. The amplitude and the phase, corresponding to this frequency, are directly computed from the Fourier function. We however initiated the process by removing the set of five frequencies composed, notably, of the two highest peaks found in the periodogram (f = 0.82 and f = 1.64 d^{-1}) and the frequencies belonging to this set. Since the frequency f = 0.82 d^{-1} presents possible harmonics, we decided to perform the fit on all of them together, taking into account the existing correlation between the power at the different frequencies. We thus designed a generalized periodogram that gives at each frequency the power included in a frequency and *its harmonics*. The method is based on a particular case of the extension of the HMM method proposed by Gosset et al. (2001). The generalized periodogram exhibits the f = 0.82 d^{-1} peak characterized by the natural width, thus further confirming that this sequence of peaks are indeed true harmonics. These frequencies were removed altogether from the data. Next, the semi-amplitude spectrum has

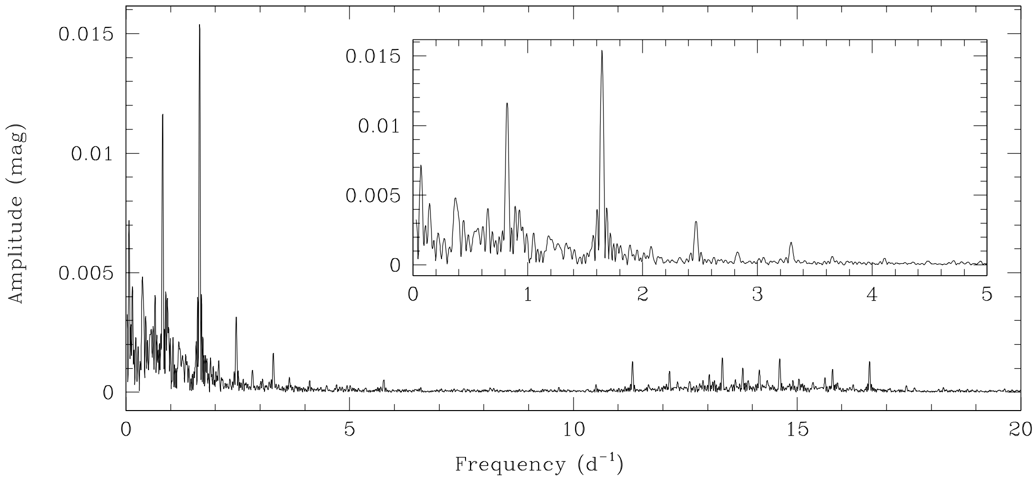

Fig. 3. Semi-amplitude spectrum of the light curve of Plaskett's star computed by the HMM method from the unflagged CoRoT data. We clearly see the aliases due to the orbital period of the satellite near 11–17 d^{-1}. The inset shows a zoom-in on the semi-amplitude spectrum in the low-frequency domain.

been computed again to detect the new highest peak to remove. The analysed data are prewhitened for this frequency and we repeated this process until reaching the noise level of the data. Figure 4 compares the semi-amplitude spectra of the data and of the data prewhitened for the first 20, the first 40 and the first 60 frequencies.

Although efficient, the iterative removing of several frequencies one by one by using the basic HMM method cannot be the final procedure. Because the light curve presents gaps and the sampling is irregular, the height of a peak is dependent on the height of other peaks in the periodogram. Therefore, we need to fit all the listed frequencies together. For this purpose, we used the extension of the HMM Fourier method to the multifrequency adjustment, a high-order Fourier method introduced by Gosset et al. (2001, their Eqs. (A13) to (A19)). Because of an excessive computation time, we applied the multifrequency analysis to binned data to be able to deal with some amount of frequencies at the same time. Indeed, since no peak is clearly dominant above 10 d^{-1}, we binned the data with a step of one twentieth of a day, i.e., with a pseudo-Nyquist frequency of $f_{\rm Ny}$ = 10 d^{-1}, reducing the CoRoT light curve into a set of 684 points. The multifrequency algorithm thus takes into account the mutual influence of the different frequencies and investigates inside the natural widths of the individual selected peaks several positions, i.e., refined values for each of the frequencies to find the current best fit.

The results obtained by both methods confirm the detection in the semi-amplitude spectrum of a first structure composed of a main frequency and six harmonics. The fundamental peak is situated around 0.823 d^{-1} and its harmonics around 1.646 d^{-1}, 2.469 d^{-1}, 3.292 d^{-1}, 4.115 d^{-1}, 4.938 d^{-1}, and 5.761 d^{-1}, respectively. Furthermore, we also clearly detect the peak corresponding to the orbital period of Plaskett's star ($f \sim 0.069$ d^{-1}) as well as two harmonics of this frequency. We also report the detection of two frequencies, actually unresolved, at f = 0.368 d^{-1} and f = 0.399 d^{-1}.

The set of frequencies computed in this way represents the final set (listed in Appendix). We stopped the iterative multifrequency procedure when the noise level was reached (statistically). This critical level is particularly difficult to estimate and constitutes the main topic of the next section.

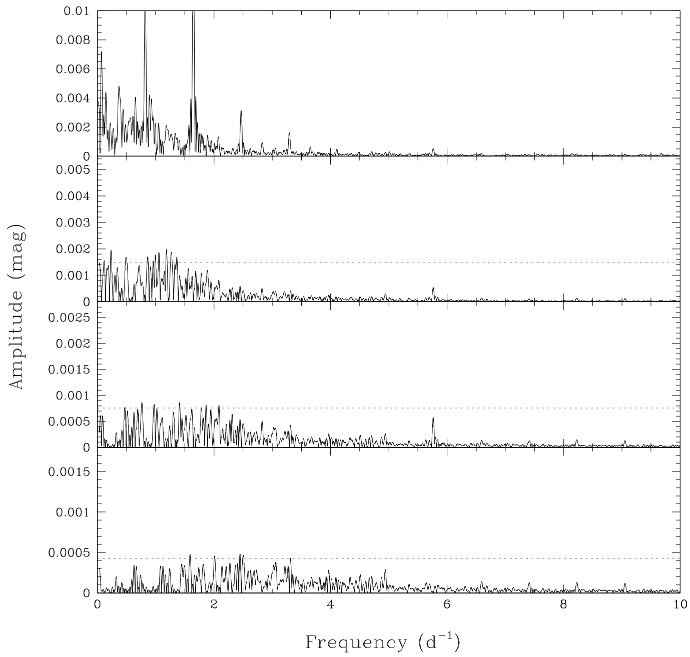

Fig. 4. For comparison, the top panel shows the semi-amplitude spectrum before prewhitening, the subsequent panels represent the semi-amplitude spectrum after prewhitening 20, 40, and 60 frequencies, respectively. The red lines exhibit the critical level at the significance level of 0.01 under a null hypothesis of white noise.

3.2. The noise properties and significant frequencies

From the analysis of the time series illustrated in Figs. 3 and 4 we conclude that there is a clear excess of power at low frequencies. It represents either the reality of the underlying deterministic signal or that the signal is partly made of red noise, i.e., is partly stochastic. Visible on the log-log plot (Fig. 5) of the periodogram of Plaskett's star, this excess of power at low frequencies ($\log f \leq 0.6$) can be described for example as suggested by Stanishev et al. (2002), by using a function of the form

$$P(f) = \frac{C}{1 + (2\pi\tau f)^{\gamma}}, \tag{1}$$

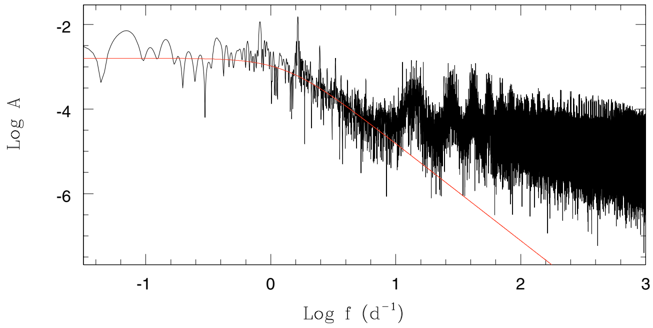

Fig. 5. Log-log plot of the semi-amplitude spectrum of Plaskett's star. The red curve represents the fitted function (Eq. (1)).

with γ related to the slope of the linear part and τ an estimation of the mean duration of the dominant transient structures in the light curve. A least-square fit of the semi-amplitude spectrum in the low-frequency domain yields the parameters $\gamma = 2.3$ and $\tau = 0.12$ d^{-1}. Assuming an origin at least partly intrinsic to the star, several processes could explain the behaviour of the stochastic component of the signal. It could be either due to an onset of clumping at the stellar photosphere or, if we make the parallelism with the works of Harvey (1985) and Aigrain et al. (2004) in helioseismology, to some kind of granulation. Indeed, Cantiello et al. (2009) suggested that the convection zone induced by the iron opacity bump can have an impact on the stellar surface behaviour and thus could be responsible for the existence of red noise. Belkacem et al. (2010) further suggested that this iron convection zone could generate stochastically excited modes in massive stars. Finally, other alternatives are also mentioned to explain this origin as the non-linearity (for more details, see e.g., Perdang 2009).

Despite the possible presence of red noise, it is therefore important to check whether peaks detected in the semi-amplitude spectrum could result from random variations rather than representing a periodic signal. However, the evaluation of the absolute significance of a peak in a periodogram of a time series with an uneven sampling is a controversial problem (e.g., Rauw et al. 2008; Frescura et al. 2008). Furthermore, the detection threshold level will be affected by this assumption of coloured noise, making its estimate more difficult. As a first order indication, we therefore applied a statistical test to establish whether the frequencies are significant, especially for those with smaller amplitudes. The probability that the power at several inspected frequencies exceeds a threshold z under the null hypothesis of a stochastic process of variance σ_f^2 (function of frequencies) is given by the empirical formula of Gosset (2007):

$$\mathrm{Prob}[Z_{\max} > z] = 1 - \left(\mathrm{e}^{-\mathrm{e}^{-0.93z+\ln(0.8N_0)}}\right), \tag{2}$$

where $Z_{\max} = \max_{0<f<f_{\rm Ny}} Z(f)$, $z = P_f/\sigma_f^2$ with P_f the power in the power spectrum at the frequency f, which is related to the semi-amplitude by $P_f = N_0 A_f^2/4$ and N_0 represents the number of datapoints. Although this expression is only adapted to even sampling, it remains a good approximation (since no better alternative exists) for uneven ones, especially for the CoRoT sampling, which is more reminiscent of a regular but gapped one. We adopted the number of datapoints in the binned light curve, i.e., $N_0 = 684$. A first estimation of the significance level can be made by adopting a null hypothesis of white noise (i.e., σ_f^2 not depending on f). In this case, we detect 79 frequencies (60 frequencies) at a significance level of 0.01 (0.001) or lower.

Table 1. Table of main frequencies.

n	Freq. (d^{-1})	Semi-Ampl. (mmag)	SL$_{\rm White}$	SL$_{\rm red}$	Comments
2	1.646	15.413	0.000	0.000	$2f_2$
1	0.823	11.373	0.000	0.000	
8	0.069	6.660	0.000	0.000	
11	0.368	5.026	0.000	0.000	
12	0.650	3.732	0.000	0.000	
9	0.139	3.410	0.000	0.000	$2f_3$
3	2.469	3.124	0.002	0.000	$3f_2$
15	0.932	3.121	0.000	0.000	
16	0.441	3.099	0.000	0.000	
14	0.888	3.069	0.000	0.000	
13	0.399	3.007	0.000	0.000	
17	0.542	2.620	0.000	0.000	
18	0.799	2.567	0.000	0.000	
21	0.572	2.524	0.000	0.000	
20	0.607	2.406	0.000	0.000	
22	1.212	2.042	0.000	0.000	
23	1.185	1.904	0.000	0.000	
28	1.264	1.877	0.000	0.000	
24	1.056	1.864	0.000	0.000	
30	1.334	1.786	0.000	0.000	
27	1.000	1.616	0.000	0.007	
32	1.359	1.598	0.000	0.000	
4	3.292	1.533	1.000	0.000	$4f_2$
33	1.558	1.362	0.000	0.000	
37	1.890	1.124	0.000	0.000	
38	1.686	1.079	0.000	0.000	
46	1.865	0.860	0.000	0.000	
47	2.085	0.834	0.000	0.000	
63	2.312	0.576	0.001	0.001	
7	5.761	0.525	1.000	0.000	$7f_2$
68	2.825	0.510	0.001	0.000	Alias + f_2?
69	2.446	0.496	0.001	0.004	
71	2.503	0.463	0.002	0.009	
74	3.314	0.425	0.004	0.000	
76	3.061	0.386	0.013	0.000	
5	4.115	0.350	1.000	0.000	$5f_2$
6	4.938	0.275	1.000	0.000	$6f_2$
95	3.969	0.256	0.110	0.000	
102	4.508	0.225	0.197	0.000	
106	4.709	0.204	0.366	0.000	
115	4.881	0.182	0.411	0.000	
148	5.646	0.133	0.298	0.000	
150	5.698	0.127	0.412	0.001	

A second approach is to adopt a more complex stochastic process as null hypothesis. In this case, we defined a stochastic distribution law by assuming an empirical function based on white noise above $f = 6.3$ d^{-1} and on red noise defined by the continuum in the power spectrum below $f = 6.3$ d^{-1}. We normalized the above fitted function in order to define a properly scaled σ_f^2 function. Under this refined null hypothesis of red noise, the number of significant frequencies decreases to about 43 (38) at a significance level of 0.01 (0.001). Table 1 exhibits the details of the significant frequencies detected under the null hypothesis of red noise. The columns represent the sequence number of the frequency, the frequency itself, its amplitude, the significance level under the null-hypothesis of white and red noise and some comments, respectively.

If we look at the evolution of the data variance with the iterative prewhitening process (Fig. 6), we note that there is no jump in the curve, which underlines the difficulty to define a threshold. Indeed, both structures formed by the fundamental peaks at

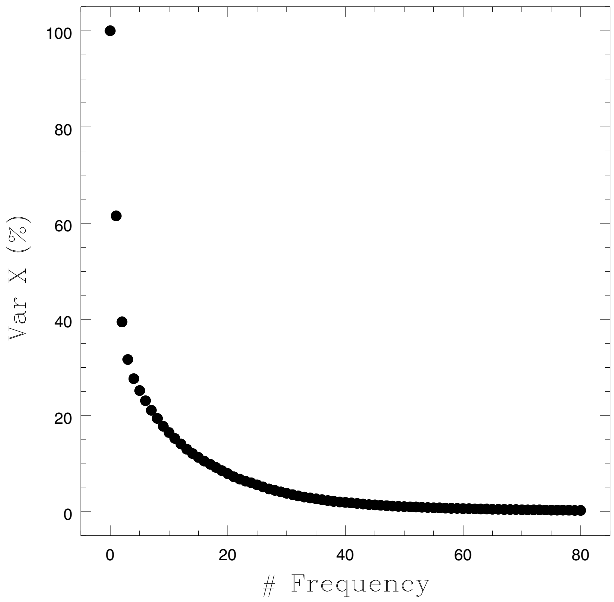

Fig. 6. Evolution of the relative variance of the prewhitened data as a function of the number of frequencies already detected by the multi-periodic algorithm.

$f = 0.823$ and $f = 0.069$ d^{-1} already explain 72% of the variance of the CoRoT light curve and, after 20 frequencies, the total variance of the prewhitened observations strongly decreased.

The decomposition of the signal into frequencies is a formal process that does not necessarily represent the physical truth. Moreover, it neglects non-linearities and complex phenomena. It is thus impossible to derive a list of frequencies free of contaminations. However, the truly existing frequencies (orbit, possible pulsations,...) should be part of this derived list (reported in the appendix). We also decided to use an additional method to contribute to the determination of the reliable frequencies, although this method is not perfect either. We split the data into two halves: a first one gathering the observations taken between HJD = 4 748.48 and 4 765.63 and a second one taking into account the data collected between HJD = 4 765.63 and 4 782.82. We applied the frequency research on each sample separately by using the same technique as above and we directly compared both frequency lists. This method allowed us to put forward a list of 30 frequencies common to both dataset.

The error estimate for the frequencies (listed in the appendix) is obtained from the expression given by Lucy & Sweeney (1971) and Montgomery & O'Donoghue (1999):

$$\epsilon(f) = \frac{\sqrt{6}}{\pi} \cdot \frac{\sigma}{\sqrt{N_0}\Delta T} \cdot \frac{1}{A}, \qquad (3)$$

where σ is the standard deviation of the residuals, A expresses the semi-amplitude associated to the frequency, ΔT represents the observation span of time and N_0, the number of points of the binned sample (684). However, these formal errors are often underestimated compared to the actual ones (Degroote et al. 2009). The list of frequencies given in the Appendix contains 150 values and was stopped at the last significant (<0.01) frequency. The first 19 frequencies are highly significant against both null hypotheses (white and red noise), but are also present in both partitional datasets.

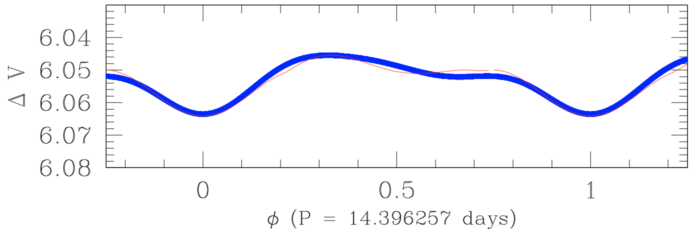

Fig. 7. Example of a model fit of the orbital part of the light curve of Plaskett's star. The parameters of the model (red thin curve) are $i = 67°$, fill$_P$ = 0.54, fill$_S$ = 0.450, longitude of the spot = 350°, radius of the spot = 7° and temperature ratio (spot/primary star) = 1.97.

4. Discussion

4.1. The inclination of the orbit of Plaskett's star

Even though the variations between the maximum and minimum observed in the entire run are close to ~0.1 mag, the unprecedented quality of the CoRoT light curve gives us enough information to attempt a study of the inclination of Plaskett's star. For this purpose, we use the NIGHTFALL programme[1] to fit the variations due to the orbital motion. This programme is based on a generalized Wilson-Devinney method assuming a standard Roche geometry.

We used the information from our Fourier analysis by combining the amplitudes and phases of the peaks detected at the orbital frequency and its first two harmonics ($f = 0.139$ and $f = 0.208$ d^{-1}). The photometric variations of HD 47129 tied to the orbital cycle have a peak-to-peak amplitude of about 19 mmag. The orbital light curve displays a broad minimum roughly centred on phase 0.0 (the conjunction with the primary star is in front)[2]. This is followed by a broad maximum around phase 0.3, whilst there is no clear secondary minimum, but rather a kind of plateau before the brightness decreases towards phase 0.0. These variations are clearly not due to grazing eclipses and cannot be explained by the sole effect of ellipsoidal variations either. Indeed, pure ellipsoidal variations in a system with a circular orbit, such as Plaskett's star, would produce a light curve with two equally deep minima centred on phases 0.0 and 0.5. We note that ellipsoidal variations in an eccentric binary could potentially account for the observed light curve (see e.g. the case of Tr 16-112, Rauw et al. 2009). However, the radial velocity curves of Plaskett's star (Linder et al. 2008, and references therein) provide no evidence whatsoever for a non-zero eccentricity. An alternative possibility to account for the shape of the orbital light curve of Plaskett's star is to assume a configuration where one of the stars has a hot spot on its surface. Indeed, the presence of such a hot, and hence bright, region could counterbalance the small ellipsoidal variations. We fitted the light curve of Plaskett's star with the following assumptions: the mass ratio as well as the temperatures of the stars are fixed according to the results of Linder et al. (2008). A priori, the hot spot could be located on the surface of either star. However, to fit the observed light curve, a spot on the secondary would have to be on the rear side of the

[1] For details, see the NIGHTFALL User Manual by Wichmann (1998) available at the URL: http://www.hs.uni-hamburg.de/DE/Ins/Per/Wichmann/Nightfall.html

[2] With respect to the time of phase 0.0 defined in Linder et al. (2008), the minimum of the light curve is shifted by about 0.03 in phase. This is somewhat larger than what can be accounted for by the uncertainty on the orbital period quoted by Linder et al. Here we have chosen to take phase 0.0 at the time of the minimum of the light curve.

star (i.e. turned away from the primary), whilst a spot on the primary star would be located on the side of the star facing the secondary. The latter configuration seems more plausible, especially in comparison with the wind interaction model of Linder et al. (2008). We therefore assume that the hot spot lies on the surface of the primary. The secondary is taken to rotate asynchronously with a rotation period one quarter of the orbital period, although we stress that this assumption has little impact on our results. At first, the inclination, the Roche lobe filling factors of both stars, the longitude of the hot spot, its radius and temperature ratio are taken as free parameters. The small amplitude of the light curve prevents us, however, from deriving strong constraints on the values of all these parameters. This dilemma can be illustrated by considering for instance the orbital inclination. As a matter of fact, when systematically exploring the parameter space, we find equally good fits for values of i ranging from 30° to 80°. Obviously to reproduce the observed light curve with $i = 80°$ requires extremely low filling factors of at least one of the stars, and this is unlikely because the spectroscopic investigation revealed a luminosity ratio of about 1.9 for stars with essentially identical temperatures (see Linder et al. 2008). Conversely, the lower inclination solutions yield unrealistically large masses. When we constrain the filling factors in a way as to reproduce the spectroscopic luminosity ratio, we find the best fit for an inclination of about 67°. Whilst this number seems quite "reasonable", we stress that it must be taken with caution. We also attempt to fit the ellipsoidal variations individually (i.e., limiting ourselves to the double of the orbital frequency and not accounting for a spot) but, once again, no exact determination of the inclination has been possible. Indeed, the fit of this parameter is directly dependent on the filling factor of both stars.

For all solutions that we find, the longitude of the bright spot is found between 345° and 355° (0° corresponding to the direction of the secondary star and 90° indicating the direction of the motion of the primary). Furthermore, this spot has a temperature ratio of about 1.9 with respect to the surface temperature of the primary. The radius of the spot is found to be about 8°–10° for most solutions, except for those with very high orbital inclinations and low filling factors.

A major problem concerning Plaskett's star remains the distance at which the binary system is situated. Indeed, whatever the configuration used to fit the light curve, the parameters used by `NIGHTFALL` indicate that the star should be located between 2.0 and 2.2 kpc. The increase of the distance would imply that Plaskett's star does not belong to the Mon OB2 association, as was already suspected by Linder et al. (2008). These authors indeed found a discrepancy between the spectral types of both stars and their dynamical masses. If we compare the systemic velocity of Plaskett's star, estimated at 30.6 ± 1.8 km s^{-1} by Linder et al. (2008), with the radial velocities of other O-type stars situated in Mon OB2 association (Mahy et al. 2009), it appears that these values agree between each other and that Plaskett's star would belong to this association. However, this assumption will can only be checked with measurements from the future Gaia mission.

In summary, whilst the light curve does not allow us to establish the inclination of the orbit, we find that its shape is consistent with moderate ellipsoidal variations altered by the presence of a rather bright spot on the primary star, facing the secondary. This spot is very probably related to the wind interaction between the two stars and could actually be due to shock-heated material that is cooling whilst it flows away from the stagnation point.

4.2. Structures present in the light curve

The multiperiodic analysis of the CoRoT light curve allowed us to detect a significant structure composed of a fundamental frequency ($f = 0.823$ d^{-1}) and its six harmonics, but the nature of this signal is not yet established.

In a binary system such as Plaskett's star, a possible cause of spectroscopic or photometric variability could be the asynchronous rotation. Indeed, a binary system is in synchronous rotation when the angular rotation velocity ω and the angular velocity of orbital motion Ω are equal. In HD 47129, this is clearly not the case: adopting the projected rotational velocities and stellar radii from Linder et al. (2008), we estimate rotational periods of about 10.3 (0.1 d^{-1}) and 1.7 days (0.6 d^{-1}) for the primary and secondary, respectively. As a result of asynchronous rotation, tidal interactions may create non-radial oscillations (Willems & Aerts 2002; Moreno et al. 2005; Koenigsberger et al. 2010). These oscillations produce a pattern of azimuthal velocity perturbations superposed on the unperturbed stellar rotation field. These tidal flows lead to the dissipation of energy owing to the viscous shear, thereby impacting on the surface temperature (and hence brightness) distribution. The azimuthal velocity components of tidal interactions are expected to produce a strong line profile variability that resembles the typical signature of non-radial pulsations (bumps in the line profile that migrate from the blue wing of the spectral lines to the red wing). The most spectacular effects are expected in eccentric binary systems, and this model was successfully used to explain the line profile variability of the eccentric B-type binary α Virginis (Moreno et al. 2005; Koenigsberger et al. 2010). Simulations of the influence of the tidal effects on the radial velocities were shown by Willems & Aerts (2002).

In a binary system with a circular orbit, the non-synchronous rotation induces variations of the radius of the non-synchronous rotating component with a super-orbital period that is longer than both the orbital and the rotational period (Moreno et al. 2005). Whilst these super-periods could leave a photometric signature, they should not be visible in the line profile variability, which is mostly dominated by the azimuthal velocity component. Moreno et al. (2005) found that in the circular non-synchronous case, the line profiles should only display a few rather broad bumps. The skewness of the line profile and its radial velocity (compared to the unperturbed profile) should display two maxima and minima per orbital cycle. The corresponding frequency should thus be twice the orbital frequency which is different from $f = 0.823$ d^{-1}.

We then consider that the structure composed of seven frequencies could be due to the rotation of one component of the binary system. In this context, we clearly see by adopting the rotational periods from Linder et al. (2008) that this set of frequencies is unlikely to correspond to the rotation of one star. A similar conclusion is expected if we take into account the projected rotational velocity evaluated by Linder et al. (2008) for both stars at about 75 km s^{-1} and 310 km s^{-1} for the primary and secondary component, respectively. Indeed, Bagnuolo et al. (1992) derived the radii from the luminosities and the effective temperatures of both stars. They found values close to 14.7 $R_\odot$ and 9.7 $R_\odot$ for the primary and secondary stars, respectively. We estimate a rotational period of about 9.9 days and 1.6 days for the primary and secondary stars, respectively, corresponding to rotational frequencies of about 0.1 d^{-1} and 0.6 d^{-1}. Alternatively, if we adopt the theoretical values of the radii quoted by Martins et al. (2005) as a function of the spectral type of each component, we obtain 21.1 $R_\odot$ and 14.2 $R_\odot$ for the primary and secondary stars, respectively, by assuming that the system is composed of an O8 I and an O7.5 III star. These values yield a rotational period of 14.2 days for the primary and 2.4 days for the secondary. These results suggest that the primary could be in synchronous rotation, while this is clearly not the case for the secondary, which would have a rotational frequency of about 0.42 d^{-1}. In both cases, it appears therefore that the fundamental frequency found in the Fourier analysis is not representative of a rotational motion, except if we could invoke a spotted surface for the secondary. But, in this case, the lack of odd multiples of the rotation frequency would be surprising. By assuming a rotational frequency of $f = 0.823$ d^{-1}, we would obtain a radius of about 7.2 $R_\odot$ for the secondary star, which seems unrealistic for these stars. However, it is possible that the frequency at $f = 0.368$ d^{-1} or $f = 0.399$ d^{-1} is representative of the rotational period of the secondary component. In the latter case, the equatorial radius of the secondary star could be estimated close to 16.7 $R_\odot$ or 15.4 $R_\odot$, respectively.

Next, we suppose that this group of frequencies could arise from wind interactions. Wiggs & Gies (1992) reported on variations of the strength of the high-velocity wings of the Hα and He I λ6678 emission line profiles. The total equivalent width of the blue and red wings of Hα was found to display a roughly recurrent modulation with a time scale of 2.82 days (0.35 d^{-1}), although the sampling of the spectra of Wiggs & Gies (1992) is admittedly not sufficient to characterize such rapid variations. These authors attributed the variations to instabilities of a radiatively cooling wind-wind interaction. It is interesting to note that this frequency is very close to the "broad peak" detected in the analysis of our photometric data (Sect. 3.1). It has to be stressed though that the *XMM-Newton* observations of Linder et al. (2006) did not reveal any indication of X-ray variability that could be related to the existence of such instabilities in the wind interaction zone.

Finally, we consider that these frequencies could be generated by non-radial pulsations. Indeed, massive stars are composed of a convective core and a radiative envelope, and gravity as well as acoustic modes can be excited (Aerts et al. 2010). Generally, for massive stars situated on the main-sequence band, the p-modes propagate with periods of a few hours while the g-modes have longer periods, of the order of days. However, for Plaskett's star, Linder et al. (2008) concluded that it is an evolved system in a post-Roche lobe overflow evolutionary stage. The inner structure of these stars is different from main-sequence stars, which decreases the g-modes periods and at the same time increases the p-modes periods (Handler 2005). Another family of modes, the strange modes (Saio et al. 1998), could also play a role in the interpretation of this structure of frequencies. These modes are known to have a propagation zone near the surface of massive stars. The exact determination of these modes requires theoretical models to predict variations produced by non-radial pulsations in a rapidly rotating massive star as well as an intense spectroscopic monitoring to characterize the variability of the line profiles. However, for Plaskett's star, massive main-sequence star models computed with ATON (Ventura et al. 2008) and an initial metallicity of 0.015, a range of mass between 30 and 70 $M_\odot$, and different mass-loss rates show that non-radial pulsations with frequency of the order of 0.8 d^{-1} can indeed be found. This frequency could be generated by modes with $l = 2, 3$, or 4.

In summary, we conclude that the alternative scenarios linked to rotation or to winds in both stars fail to explain the structure of the Fourier spectrum, especially the dominant frequency and its set of harmonics. The assumption of multiperiodic non-radial pulsations remains the most plausible one to understand the low-frequency variability detected in the CoRoT light curve of Plaskett's star.

5. Conclusions

We presented the photometric analysis of the very massive binary system HD 47129 observed by CoRoT during the second run SRa02 (~34.33 days). The light curve shows indications of intrinsic variations of the stars, providing evidence of a large number of frequencies. We extracted a total of about 43 frequencies (Table 1), significant under a null hypothesis of red noise, by using two different techniques based on a standard prewhitening and a multiperiodic algorithm. We emphasize that all the frequencies, reported in the present paper, have not necessarily a physical meaning.

This analysis highlighted a group consisting of one fundamental frequency (0.823 d^{-1}) and its six harmonics. In addition, a second structure formed by the orbital frequency (0.069 d^{-1}) and its two harmonics allowed us to investigate the light variation due to orbital effects. This analysis revealed the presence of a hot spot, probably located near the primary star, facing the secondary component and having an origin in the colliding wind interaction zone. However, the determination of the exact value of the system inclination turned out to be ambiguous. A third structure, formed by a much wider peak and thus certainly composed of two frequencies at 0.368 d^{-1} and 0.399 d^{-1}, has also been detected. One of these frequencies could be related to the rotation of the secondary even though Wiggs & Gies (1992) rather suggested an origin in the winds of the stars.

The future work will be devoted to the interpretation of these frequencies in terms of asteroseismology in order to remove an additional part of mystery concerning Plaskett's star. Moreover, a study of the line profiles either of the secondary or of the primary component, obtained from an intense high-resolution spectroscopic campaign, could provide further constraints on the properties of the pulsation modes. Indeed, the broad and shallow line profiles of the secondary star favour this detection, although the orbital motion and the presence of the primary star will certainly render this task more difficult.

Acknowledgements. We thank the CoRoT team for the acquisition and the reduction of the CoRoT data. This present work was supported by the FNRS (Belgium), the PRODEX XMM/Integral contract (Belspo), Gaia DPAC Prodex and the Communauté française de Belgique – Action de recherche concertée – ARC – Académie Wallonie-Europe. The research leading to these results has also received funding from the European Research Council under the European Community's Seventh Framework Programme (FP7/2007–2013)/ERC grant agreement No. 227224 (PROSPERITY), from the Research Council of K.U. Leuven (GOA/2008/04), and from the Belgian federal science policy office (C90309: CoRoT Data Exploitation). M.G. and A.N. thank J. Montalban and P. Ventura for help in computation aspects of massive stars.

References

Aerts, C., Christensen-Dalsgaard, J., & Kurtz, D. W. 2010, Asteroseismology (Springer)
Aigrain, S., Favata, F., & Gilmore, G. 2004, A&A, 414, 1139
Auvergne, M., Bodin, P., Boisnard, L., et al. 2009, A&A, 506, 411
Baglin, A., Auvergne, M., Barge, P., et al. 2006, in ESA SP, ed. M. Fridlund, A. Baglin, J. Lochard, & L. Conroy, 1306, 33
Bagnuolo, Jr., W. G., Gies, D. R., & Wiggs, M. S. 1992, ApJ, 385, 708
Belkacem, K., Dupret, M. A., & Noels, A. 2010, A&A, 510, A6
Cantiello, M., Langer, N., Brott, I., et al. 2009, A&A, 499, 279
Degroote, P., Aerts, C., Ollivier, M., et al. 2009, A&A, 506, 471
Ferraz-Mello, S. 1981, AJ, 86, 619
Frescura, F. A. M., Engelbrecht, C. A., & Frank, B. S. 2008, MNRAS, 388, 1693
González, J. F., & Levato, H. 2006, A&A, 448, 283

Gosset, E. 2007, Le calcul du niveau de signification du plus haut pic dans les périodogrammes de type Fourier par la formule de Horne-Baliunas est contre-indiqué, Thèse d'Agrégation de l'Enseignement Supérieur, Seconde Thèse Annexe, University of Liège
Gosset, E., Royer, P., Rauw, G., Manfroid, J., & Vreux, J.-M. 2001, MNRAS, 327, 435
Handler, G. 2005, JApA, 26, 241
Harvey, J. 1985, in Future Missions in Solar, Heliospheric & Space Plasma Physics, ed. E. Rolfe, & B. Battrick, ESA SP, 235, 199
Heck, A., Manfroid, J., & Mersch, G. 1985, A&AS, 59, 63
Hillier, D. J., & Miller, D. L. 1998, ApJ, 496, 407
Howarth, I. D., & Reid, A. H. N. 1993, A&A, 279, 148
Kambe, E., Hirata, R., Ando, H., et al. 1997, ApJ, 481, 406
Koenigsberger, G., Moreno, E., & Harrington, D. M. 2010, 425, 209
Linder, N., Rauw, G., Pollock, A. M. T., & Stevens, I. R. 2006, MNRAS, 370, 1623
Linder, N., Rauw, G., Martins, F., et al. 2008, A&A, 489, 713
Lucy, L. B., & Sweeney, M. A. 1971, AJ, 76, 544
Mahy, L., Nazé, Y., Rauw, G., et al. 2009, A&A, 502, 937
Martins, F., Schaerer, D., & Hillier, D. J. 2005, A&A, 436, 1049
Montgomery, M. H., & O'Donoghue, D. 1999, Delta Scuti Star Newsletter, 13, 28
Moreno, E., Koenigsberger, G., & Toledano, O. 2005, A&A, 437, 641
Morrison, N. D. 1978, PASP, 90, 493
Perdang, J. 2009, in EAS PS, ed. M. Goupil, Z. Koláth, N. Nardetto, & P. Kervella, 38, 43
Rauw, G., De Becker, M., van Winckel, H., et al. 2008, A&A, 487, 659
Rauw, G., Nazé, Y., Fernández Lajús, E., et al. 2009, MNRAS, 398, 1582
Reese, D. R., Thompson, M. J., MacGregor, K. B., et al. 2009, A&A, 506, 183
Rudy, R. J., & Herman, L. C. 1978, PASP, 90, 163
Saio, H., Baker, N. H., & Gautschy, A. 1998, MNRAS, 294, 622
Scargle, J. D. 1982, ApJ, 263, 835
Stanishev, V., Kraicheva, Z., Boffin, H. M. J., & Genkov, V. 2002, A&A, 394, 625
Ventura, P., D'Antona, F., & Mazzitelli, I. 2008, Ap&SS, 316, 93
Wichmann, R. 1998, Nightfall User Manual
Wiggs, M. S., & Gies, D. R. 1992, ApJ, 396, 238
Willems, B., & Aerts, C. 2002, A&A, 384, 441

Pages 10 to 12 are available in the electronic edition of the journal at http://www.aanda.org

Table 2. Total list of frequencies. The errors given on the frequencies, semi-amplitudes and phase correspond to the 1-σ error. The T_0 of the phase is equal to 2 450 000. The last column marks the frequencies present both in the first part of the light curve and in the second one.

n	Frequency (d^{-1})	Frequency errors (d^{-1})	Semi-Ampl. (mmag)	Semi-Ampl. errors (mmag)	Phase (rad)	Phase errors (rad)	Variance $\times 10^{-4}$	SL_{white}	SL_{red}	Present in both halves
1	0.823	0.001	11.373	0.949	–1.220	0.083	3.080995	0.0000	0.0000	*
2	1.646	0.001	15.413	0.842	–0.622	0.055	2.423326	0.0000	0.0000	*
3	2.469	0.003	3.124	0.601	–0.747	0.192	1.235682	0.0019	0.0000	*
4	3.292	0.006	1.533	0.589	0.220	0.384	1.185302	1.0000	0.0000	*
5	4.115	0.027	0.350	0.586	–0.037	1.673	1.174480	1.0000	0.0000	*
6	4.938	0.034	0.275	0.586	–0.965	2.130	1.173976	1.0000	0.0000	*
7	5.761	0.018	0.525	0.586	0.982	1.116	1.173613	1.0000	0.0000	*
8	0.069	0.001	6.660	0.585	–1.084	0.088	1.172099	0.0000	0.0000	*
9	0.139	0.002	3.410	0.522	1.335	0.153	0.931321	0.0000	0.0000	*
10	0.208	0.008	1.069	0.505	–1.284	0.472	0.871496	1.0000	1.0000	*
11	0.368	0.002	5.026	0.503	–1.213	0.100	0.865742	0.0000	0.0000	*
12	0.650	0.002	3.732	0.468	1.264	0.125	0.748715	0.0000	0.0000	*
13	0.399	0.002	3.007	0.442	0.230	0.147	0.667486	0.0000	0.0000	*
14	0.888	0.002	3.069	0.421	–0.513	0.137	0.607357	0.0000	0.0000	*
15	0.932	0.002	3.121	0.403	–0.309	0.129	0.555454	0.0000	0.0000	*
16	0.441	0.002	3.099	0.388	–1.337	0.125	0.513773	0.0000	0.0000	*
17	0.542	0.002	2.620	0.373	–0.173	0.142	0.474797	0.0000	0.0000	*
18	0.799	0.002	2.567	0.359	–1.020	0.140	0.439750	0.0000	0.0000	*
19	0.270	0.003	2.031	0.345	–0.856	0.170	0.406977	0.0001	0.0731	*
20	0.607	0.002	2.406	0.333	0.687	0.138	0.378262	0.0000	0.0002	
21	0.572	0.002	2.524	0.321	1.521	0.127	0.353378	0.0000	0.0001	
22	1.212	0.002	2.042	0.309	–1.481	0.151	0.327324	0.0000	0.0000	*
23	1.185	0.003	1.904	0.299	0.573	0.157	0.304987	0.0000	0.0000	
24	1.056	0.002	1.864	0.289	0.991	0.155	0.285933	0.0000	0.0000	*
25	0.234	0.002	1.874	0.280	1.442	0.150	0.268622	0.0000	0.2550	
26	0.492	0.002	1.798	0.271	–0.749	0.151	0.251324	0.0000	0.2587	
27	1.000	0.003	1.616	0.262	–0.643	0.162	0.235295	0.0000	0.0074	
28	1.264	0.002	1.877	0.254	0.034	0.135	0.220528	0.0000	0.0000	*
29	0.112	0.003	1.550	0.246	0.643	0.158	0.206262	0.0000	0.9622	
30	1.334	0.002	1.786	0.237	0.060	0.133	0.191779	0.0000	0.0000	*
31	0.860	0.002	1.552	0.229	1.343	0.147	0.178966	0.0000	0.1327	
32	1.359	0.002	1.598	0.221	–0.486	0.139	0.167517	0.0000	0.0000	
33	1.558	0.003	1.362	0.213	–0.844	0.157	0.155760	0.0000	0.0000	*
34	0.039	0.002	1.383	0.207	0.563	0.150	0.146522	0.0000	0.9999	
35	0.181	0.003	1.258	0.200	–0.344	0.159	0.137192	0.0000	1.0000	
36	0.716	0.002	1.370	0.195	0.033	0.142	0.129616	0.0000	0.9343	
37	1.890	0.003	1.124	0.189	1.140	0.168	0.122645	0.0000	0.0000	*
38	1.686	0.003	1.079	0.184	0.051	0.171	0.116239	0.0001	0.0000	
39	0.951	0.003	1.002	0.180	0.718	0.180	0.110602	0.0003	1.0000	
40	0.513	0.003	0.962	0.175	1.345	0.182	0.105189	0.0005	1.0000	
41	0.754	0.003	1.032	0.171	–1.246	0.166	0.100534	0.0000	1.0000	
42	0.835	0.003	0.970	0.167	0.723	0.172	0.095679	0.0001	1.0000	
43	1.299	0.003	0.865	0.163	0.868	0.188	0.090910	0.0011	0.8833	
44	0.158	0.003	0.848	0.160	–1.205	0.188	0.087160	0.0011	1.0000	
45	1.151	0.003	0.844	0.156	–0.048	0.185	0.083626	0.0007	1.0000	
46	1.865	0.003	0.860	0.153	0.208	0.178	0.080134	0.0002	0.0002	
47	2.085	0.003	0.834	0.150	0.148	0.180	0.076910	0.0003	0.0000	*
48	0.342	0.003	0.819	0.147	0.994	0.179	0.073469	0.0003	1.0000	
49	1.617	0.003	0.797	0.143	–1.443	0.180	0.070242	0.0003	0.1162	
50	0.626	0.003	0.785	0.140	–0.741	0.178	0.067099	0.0002	1.0000	
51	0.680	0.003	0.771	0.137	–0.905	0.177	0.064008	0.0002	1.0000	
52	0.089	0.003	0.694	0.134	–0.199	0.193	0.061305	0.0020	1.0000	
53	1.781	0.003	0.679	0.131	–1.315	0.193	0.058821	0.0021	0.1551	
54	1.412	0.003	0.656	0.128	1.270	0.196	0.056409	0.0029	1.0000	*
55	0.303	0.003	0.690	0.126	–1.245	0.182	0.054027	0.0004	1.0000	
56	0.922	0.003	0.649	0.123	–0.369	0.189	0.051694	0.0013	1.0000	
57	1.948	0.003	0.650	0.120	0.673	0.185	0.049628	0.0007	0.0324	*
58	1.524	0.003	0.641	0.118	–0.191	0.184	0.047574	0.0006	0.9958	
59	0.460	0.003	0.735	0.115	–0.261	0.157	0.045514	0.0000	1.0000	
60	0.418	0.003	0.634	0.113	0.752	0.178	0.043567	0.0002	1.0000	
61	2.044	0.003	0.585	0.110	0.785	0.188	0.041588	0.0011	0.0555	
62	1.232	0.003	0.561	0.108	0.050	0.192	0.039811	0.0019	1.0000	
63	2.312	0.003	0.576	0.106	–0.542	0.183	0.038170	0.0005	0.0011	*
64	1.086	0.003	0.612	0.103	0.959	0.169	0.036539	0.0000	1.0000	

Table 2. continued.

n	Frequency (d^{-1})	Frequency errors (d^{-1})	Semi-Ampl. (mmag)	Semi-Ampl. errors (mmag)	Phase (rad)	Phase errors (rad)	Variance $\times 10^{-4}$	SL_{white}	SL_{red}	Present in both halves
65	1.022	0.003	0.585	0.101	–0.733	0.173	0.034927	0.0001	1.0000	
66	0.653	0.003	0.520	0.099	0.338	0.190	0.033229	0.0013	1.0000	
67	1.587	0.003	0.521	0.097	0.526	0.185	0.031866	0.0007	1.0000	
68	2.825	0.003	0.510	0.095	–1.458	0.185	0.030561	0.0007	0.0000	*
69	2.446	0.003	0.496	0.093	–0.521	0.186	0.029301	0.0008	0.0045	
70	0.210	0.003	0.479	0.091	0.169	0.189	0.028069	0.0012	1.0000	
71	2.503	0.003	0.463	0.089	–0.851	0.192	0.026939	0.0017	0.0092	
72	0.979	0.003	0.431	0.087	1.115	0.202	0.025891	0.0061	1.0000	
73	2.011	0.003	0.431	0.085	–1.410	0.198	0.024960	0.0039	0.9923	
74	3.314	0.003	0.425	0.084	–0.700	0.197	0.024034	0.0035	0.0000	
75	1.816	0.003	0.399	0.082	1.367	0.206	0.023132	0.0094	1.0000	
76	3.061	0.003	0.386	0.081	0.343	0.209	0.022321	0.0135	0.0002	
77	0.599	0.003	0.390	0.079	0.078	0.203	0.021571	0.0072	1.0000	
78	1.488	0.003	0.366	0.078	1.451	0.213	0.020854	0.0193	1.0000	
79	1.120	0.003	0.382	0.077	–0.650	0.201	0.020170	0.0055	1.0000	
80	2.274	0.003	0.367	0.075	–0.571	0.205	0.019467	0.0089	0.9689	
81	1.669	0.003	0.357	0.074	–0.232	0.207	0.018776	0.0110	1.0000	
82	1.453	0.003	0.354	0.073	–1.278	0.206	0.018191	0.0097	1.0000	
83	2.136	0.003	0.336	0.072	0.383	0.214	0.017585	0.0204	1.0000	
84	0.484	0.003	0.329	0.071	–0.148	0.214	0.017009	0.0212	1.0000	
85	3.032	0.004	0.303	0.069	–0.882	0.229	0.016449	0.0752	0.0782	
86	3.219	0.004	0.303	0.068	–0.424	0.226	0.015969	0.0578	0.0115	
87	0.800	0.004	0.298	0.067	0.859	0.226	0.015523	0.0593	1.0000	
88	2.630	0.004	0.288	0.066	0.222	0.230	0.015091	0.0818	0.9744	
89	2.362	0.004	0.281	0.066	0.836	0.233	0.014691	0.0986	1.0000	
90	1.736	0.004	0.280	0.065	0.991	0.231	0.014304	0.0882	1.0000	
91	0.026	0.004	0.282	0.064	0.440	0.227	0.013914	0.0615	1.0000	
92	3.000	0.004	0.272	0.063	1.194	0.231	0.013503	0.0854	0.4292	
93	3.267	0.004	0.275	0.062	–0.866	0.225	0.013120	0.0550	0.0465	
94	2.686	0.004	0.268	0.061	–1.529	0.228	0.012741	0.0664	0.9950	
95	3.969	0.004	0.256	0.060	–0.320	0.235	0.012373	0.1103	0.0001	
96	1.377	0.004	0.250	0.059	–0.586	0.237	0.012041	0.1328	1.0000	
97	2.214	0.004	0.242	0.059	1.496	0.242	0.011721	0.1746	1.0000	
98	0.178	0.004	0.237	0.058	–0.223	0.243	0.011419	0.1929	1.0000	
99	2.734	0.004	0.249	0.057	1.000	0.229	0.011133	0.0755	0.9996	
100	0.710	0.004	0.245	0.056	–1.398	0.230	0.010865	0.0785	1.0000	
101	0.896	0.004	0.246	0.056	1.394	0.226	0.010589	0.0589	1.0000	
102	4.508	0.004	0.225	0.055	–0.565	0.244	0.010298	0.1966	0.0000	
103	1.175	0.004	0.224	0.054	0.888	0.242	0.010044	0.1736	1.0000	
104	2.571	0.004	0.223	0.054	0.064	0.240	0.009795	0.1582	1.0000	
105	2.172	0.004	0.205	0.053	–0.714	0.257	0.009551	0.3888	1.0000	
106	4.709	0.004	0.204	0.052	–0.305	0.256	0.009339	0.3664	0.0000	
107	2.758	0.004	0.201	0.052	1.071	0.257	0.009131	0.3820	1.0000	
108	3.675	0.004	0.198	0.051	0.702	0.258	0.008926	0.3961	0.3397	
109	4.092	0.004	0.201	0.051	0.846	0.252	0.008729	0.3006	0.0137	
110	3.817	0.004	0.199	0.050	1.131	0.251	0.008536	0.2862	0.1327	
111	2.417	0.004	0.192	0.049	–0.180	0.258	0.008340	0.3912	1.0000	
112	3.174	0.004	0.190	0.049	–0.642	0.257	0.008154	0.3775	0.9999	
113	1.698	0.004	0.188	0.048	–0.220	0.258	0.007975	0.3893	1.0000	
114	0.544	0.004	0.185	0.048	–1.488	0.258	0.007796	0.4052	1.0000	
115	4.881	0.004	0.182	0.047	–1.268	0.259	0.007625	0.4108	0.0001	
116	1.266	0.004	0.176	0.047	–0.486	0.265	0.007458	0.5180	1.0000	
117	4.338	0.004	0.176	0.046	1.237	0.262	0.007297	0.4611	0.0252	
118	0.399	0.004	0.169	0.046	–1.036	0.270	0.007136	0.6133	1.0000	
119	3.413	0.004	0.173	0.045	1.460	0.262	0.006993	0.4597	0.9995	
120	2.063	0.004	0.169	0.045	0.953	0.265	0.006849	0.5155	1.0000	
121	4.440	0.004	0.169	0.044	–0.939	0.262	0.006704	0.4711	0.0279	
122	1.628	0.004	0.160	0.044	–0.387	0.274	0.006564	0.6661	1.0000	
123	2.938	0.004	0.175	0.043	–0.283	0.248	0.006436	0.2508	1.0000	
124	2.600	0.004	0.163	0.043	–0.035	0.264	0.006313	0.4980	1.0000	
125	3.134	0.004	0.159	0.043	1.172	0.267	0.006186	0.5466	1.0000	
126	0.756	0.004	0.157	0.042	0.189	0.267	0.006061	0.5585	1.0000	
127	2.802	0.004	0.156	0.042	0.559	0.268	0.005942	0.5613	1.0000	
128	3.732	0.004	0.150	0.041	1.278	0.274	0.005821	0.6765	0.9990	
129	0.358	0.004	0.149	0.041	0.198	0.274	0.005706	0.6692	1.0000	

Table 2. continued.

n	Frequency (d^{-1})	Frequency errors (d^{-1})	Semi-Ampl. (mmag)	Semi-Ampl. errors (mmag)	Phase (rad)	Phase errors (rad)	Variance $\times 10^{-4}$	SL_{white}	SL_{red}	Present in both halves
130	1.326	0.004	0.149	0.040	–0.873	0.272	0.005597	0.6370	1.0000	
131	1.059	0.004	0.145	0.040	0.175	0.276	0.005486	0.7007	1.0000	
132	1.857	0.003	0.190	0.040	1.567	0.209	0.005379	0.0126	1.0000	
133	1.902	0.003	0.193	0.039	–1.303	0.204	0.005273	0.0075	1.0000	
134	1.975	0.004	0.161	0.039	–1.506	0.241	0.005137	0.1689	1.0000	
135	0.141	0.004	0.147	0.038	1.142	0.260	0.005012	0.4364	1.0000	
136	3.601	0.004	0.140	0.038	–0.660	0.270	0.004907	0.6029	1.0000	
137	6.593	0.004	0.140	0.037	–0.019	0.268	0.004809	0.5695	1.0000	
138	4.216	0.004	0.137	0.037	0.991	0.271	0.004711	0.6196	0.9020	
139	3.538	0.004	0.142	0.037	–0.623	0.259	0.004618	0.4214	1.0000	
140	8.228	0.004	0.134	0.036	–1.086	0.272	0.004529	0.6323	1.0000	
141	0.844	0.004	0.130	0.036	0.465	0.277	0.004440	0.7262	1.0000	
142	7.411	0.004	0.132	0.036	1.112	0.271	0.004353	0.6157	1.0000	
143	2.475	0.004	0.129	0.035	–1.353	0.273	0.004267	0.6604	1.0000	
144	3.774	0.004	0.133	0.035	1.255	0.262	0.004187	0.4734	1.0000	
145	3.927	0.004	0.129	0.035	0.480	0.269	0.004108	0.5867	1.0000	
146	3.370	0.004	0.126	0.034	0.044	0.273	0.004027	0.6588	1.0000	
147	3.446	0.004	0.134	0.034	0.620	0.254	0.003948	0.3289	1.0000	
148	5.646	0.004	0.133	0.034	0.178	0.252	0.003858	0.2980	0.0005	
149	1.023	0.004	0.121	0.033	–0.332	0.276	0.003782	0.7016	1.0000	
150	5.698	0.004	0.127	0.033	0.742	0.259	0.003708	0.4120	0.0012	